



Transient Chaos in the Hénon Map

Rodrigo Simile Baroni¹ · Iberê Luiz Caldas¹

Received: 17 October 2025 / Accepted: 5 January 2026
© The Author(s) 2026

Abstract

Chaos in nonlinear systems manifests as irregular, unpredictable dynamics sensitive to initial conditions. While chaotic attractors (e.g., the Lorenz butterfly) are commonly considered in research contexts, the transient is often disregarded, although its dynamics can be complex and should be taken into consideration when the average transient time is comparable to the experimental or numerical observation timescale. Using the Hénon map as a prototype, we report fundamental concepts of transient chaos. We contrast permanent and transient chaos, quantify lifetimes through survival probability analysis, and visualize their fractal phase space distribution. The stable and unstable invariant manifolds of the map's fixed points are introduced; these geometric structures are the backbones of the dynamics and compose a non-attracting invariant set, the chaotic saddle, that underlies the transient chaos. By analyzing how the system's attractors change as a control parameter varies, we identify two types of scenarios where the chaotic attractor loses stability and is replaced by a chaotic saddle: via saddle-node bifurcation and boundary crisis. We also identify an interior crisis, where the chaotic attractor absorbs the chaotic saddle, resulting in an expanded attractor. We conclude by highlighting implications on other classes of dynamical systems.

Keywords Nonlinear systems · Chaos theory · Transient chaos · Chaotic saddles

1 Introduction

In dynamical systems theory, transient dynamics correspond to the temporal evolution that precedes the asymptotic states usually referred to as attractors [1–4]. Oftentimes, in the numerical investigation of a system, the transient is disregarded and the focus is on the characterization of the attractors. However, the transient dynamics may be more relevant than the asymptotic states in terms of the observation, modeling, and control of a phenomenon. This is the case when the average lifetime of the transient is comparable to the observation time, as numerical and experimental investigations are always performed over a finite time interval.

Several experiments have produced evidence of transient chaos, such as chemical reactions preceding thermal equilibrium [5–7], the parametrically driven damped pendulum [8–10], and the emission of light from dielectric cavities [11, 12]. Another example is the convection loop experiment [13–16], which consists of a loop-shaped reservoir filled with water, heated from below and cooled from above. This is a one-dimensional analogue of the Rayleigh-Bénard convection problem, which can be described by the Lorenz model [17] for certain parameters.

The goal of this paper is to present the concept and properties of transient chaos through the Hénon map [18] as an example. Despite its simplicity, the Hénon map exhibits rich dynamical behavior and a complex bifurcation structure as its parameters vary [4, 19]. First introduced as a simplified model for a Poincaré section of the Lorenz system [18], it has become a paradigmatic system for research in fundamental and advanced topics in nonlinear dynamics.

The Hénon map is a two-dimensional, invertible, discrete time system that captures the essential dynamics of a dissipative three-dimensional flow [2]. For certain parameter values, one must iterate the map many times before trajectories settle onto the system's attractor, a

Iberê Luiz Caldas contributed equally to this work.

✉ Rodrigo Simile Baroni
r.baroni@usp.br

Iberê Luiz Caldas
ibere@if.usp.br

¹ Instituto de Física, Universidade de São Paulo - USP, São Paulo 05508-900, São Paulo, Brazil

signature of transient chaos. We demonstrate that this phenomenon arises from the existence of a non-attracting chaotic set in phase space, known as a chaotic saddle [1, 20–24].

In this work, we carry out a numerical exploration of the Hénon map across representative parameter sets that illustrate distinct dynamical behaviors. After contrasting configurations with permanent and transient chaos, emphasis is given to the invariant manifolds of unstable orbits. These geometric structures underlie the phase space and form chaotic sets that can compose either a chaotic attractor or a chaotic saddle. Segments of the manifolds are computed with a precise interpolation scheme [25], while the chaotic saddle is approximated with the Proper Interior Maximum (PIM) triple method [26], which numerically finds chaotic trajectories that remain in close vicinity to the chaotic saddle for arbitrarily long times. We analyze how varying a control parameter can induce abrupt qualitative changes in the system, known as crises [1–3, 27, 28], that create or destroy chaotic attractors and chaotic saddles. We interpret the mechanisms behind those global bifurcations in terms of manifold interactions.

The paper is organized as follows. In Section 2 we review the distinction between permanent and transient chaos and present a numerical computation of the transient lifetimes for selected parameter values. Section 3 presents the definition of stable and unstable manifolds, their role in organizing the phase space dynamics, and in the formation of chaotic sets. In Section 4 we discuss the periodic windows of the system, which, despite their name, are parameter regions where transient chaos is usually observed. We also present two types of crises and their relation to transient chaos. Finally, Section 5 presents our concluding remarks, including a discussion of the effects of chaotic saddles in complex systems, a field with broad applications; and of chaotic scattering, a manifestation of transient chaos in open conservative systems.

2 Permanent and Transient Chaos

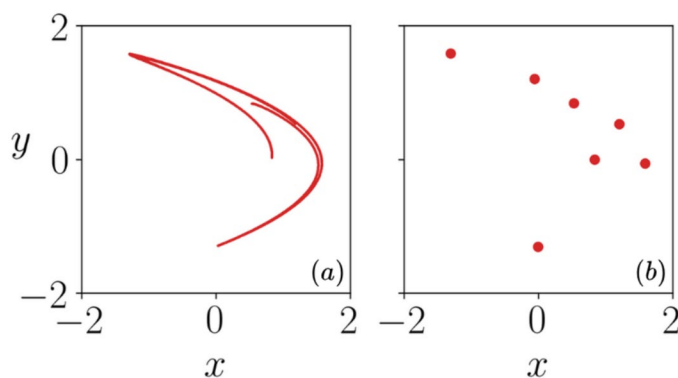
The Hénon map M is defined by the equations

$$M : \begin{cases} x_{n+1} = a + by_n - x_n^2, \\ y_{n+1} = x_n, \end{cases} \quad (1)$$

where a and b are the control parameters. It exhibits a chaotic attractor for the parameters $a = 1.22$ and $b = 0.3$, where almost all trajectories initialized in a trapping region, R , converge to a chaotic attractor, shown in Fig. 1(a). Such trajectories remain in the chaotic attractor for arbitrarily long times. In contrast, when $a = 1.23$, a period-7 attractor is observed. This is shown in Fig. 1(b), and now almost all trajectories starting in the trapping region converge to this periodic state. In both cases, trajectories starting outside of R diverge to minus infinity. The boundary of R is delimited by a stable manifold, as is discussed in Section 3. We say that *almost every* trajectory starting in the trapping region converges to the attractors because there are unstable periodic orbits inside R .

Despite the asymptotic state shown in Fig. 1(b) being a periodic attractor, its transient is chaotic. To observe the transient dynamics, Fig. 2(a) illustrates two nearby initial conditions whose 7th iterates of the x coordinate are shown. One of them, shown in blue, oscillates irregularly for approximately 400 iterations before reaching the periodic attractor, identified by a plateau since only every 7 iterates are shown. The second initial condition, shown in orange, is a small perturbation of order 10^{-15} applied to the first one. Now, it oscillates irregularly for about 100 iterations before reaching the attractor. This shows that nearby initial conditions lead to different transient lifetimes, exemplifying the sensitivity to initial condition characteristic of both permanent and transient chaos. Panel (b) shows the complete evolution in the phase space, and we see that the chaotic transient motion appears to be distributed along a defined region that resembles the chaotic attractor of Fig. 1(a) after a certain time.

Fig. 1 Attractors of the Hénon map for $b = 0.3$. (a) $a = 1.22$, chaotic attractor; and (b) $a = 1.23$, period-7 attractor



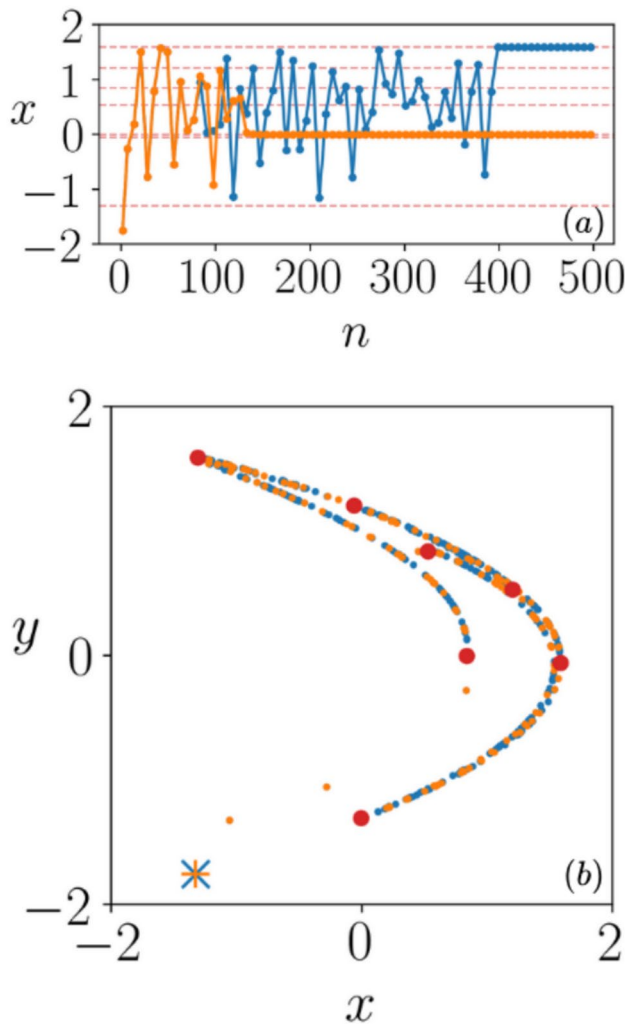


Fig. 2 (a) Time evolution of the x coordinate for two initial conditions, each seventh iteration is shown. In blue, a long-lived initial condition that reached the periodic attractor after 400 iterations. In orange, the initial condition was shifted by 10^{-15} , and a much shorter transient is observed. The x coordinates of the periodic attractor is indicated by the horizontal dashed lines. (b) Evolution of the orange and blue initial conditions, indicated by the '+' and 'x' symbols, respectively. The periodic attractor is represented by the red circles

To analyze the transient, we initialize an ensemble of $N(0)$ points uniformly in a square region of phase space, $|x| < 2$ and $|y| < 2$, excluding the attractor, and iterate each until it either escapes the initial box or falls onto the attractor. The initial conditions that escape the box diverge to infinity and are discarded. In the case of chaotic transients, the number of survivors $N(n)$ after n iterations decays exponentially,

$$N(n) \sim e^{-\kappa n}, \tag{2}$$

where κ is the escape rate [1, 29], a quantity that measures how quickly the initial conditions reach the attractor. Equation (2) indicates that the number of survivors decreases by

a factor of $1/e$ after $1/\kappa$ iterations, implying that most trajectories exhibit a transient lifetime less than $1/\kappa$. Thus, the average lifetime of the chaotic transient can be estimated as

$$\tau \approx 1/\kappa. \tag{3}$$

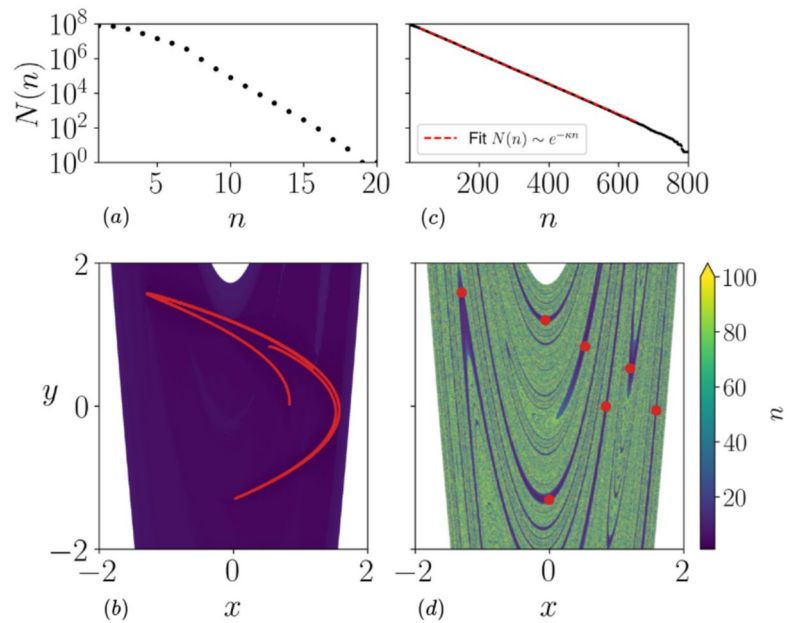
Figure 3 compares the transient lifetimes for the two parameter settings presented in Fig. 1. In panels (a) and (b), we considered $a = 1.22$, where the attractor is chaotic. Panel (a) shows the number of surviving trajectories versus the number of iterations, starting with roughly 10^8 initial points that reach the attractor with less than 20 iterations. In panel (b) we project the lifetimes onto the phase space, with the attractor shown in red. In this first example, the transient times are relatively short.

Panels (c) and (d) illustrate the case of the period-7 attractor ($a = 1.23$), for which the transient is longer and more complex. In panel (c) the survival curve shows that more than 800 iterations are necessary for the $\sim 10^8$ trajectories to reach the attractor. We note that the decay of the survival curve is not purely exponential; for very short times, there is a slower decay that depends on the number of initial conditions and the region in which they are distributed, while the tail of the curve shows strong statistical fluctuations due to having only a few survivors left. Thus, we perform an exponential fit for the intermediate times between n_{min} and n_{max} . The fitting in panel (c) considered $n_{min} = 30$ and $n_{max} = 650$, yielding the escape rate $\kappa = 0.0200553 \pm 1.8 \times 10^{-6}$ and an average transient lifetime $\tau = 49.9862 \pm 4.5 \times 10^{-3}$. This result changes slightly if the fitting window is shifted slightly. The escape rate does not depend on the ensemble of initial conditions, as it is a property of the chaotic saddle. The exponential fitting procedure with $\sim 10^6$ initial conditions resulted in $\kappa = 0.0199739 \pm 9.9 \times 10^{-6}$, and an ensemble of $\sim 10^4$ yielded $\kappa = 0.0201150 \pm 2.8 \times 10^{-5}$. Panel (d) projects the lifetimes onto the phase space and the periodic attractor is indicated by red circles. The resulting pattern is highly intricate: small shifts in initial conditions produce considerably different lifetimes, with the longest-lived trajectories filling regions close to the stable manifold, an invariant set which will be discussed in the next section.

3 Invariant Manifolds and the Chaotic Saddle

To interpret the main intermittency characteristics of the chaotic transient and explain its origin, we introduce the concepts of stable and unstable manifolds and chaotic saddles [1–3], invariant sets associated with the system’s unstable periodic orbits (UPOs).

Fig. 3 (a) and (b), number of surviving trajectories as a function of the number of iterations and projection of survival times in the phase space, for $a = 1.22$. (c) and (d), the same for $a = 1.23$; the exponential fitting in (c) furnished $\kappa = 0.0200553 \pm 1.8 \times 10^{-6}$ and $\tau = 49.9862 \pm 4.5 \times 10^{-3}$. In panels (b) and (d), the attractors are represented in red. The white region correspond to initial conditions that diverged; those were not considered when computing $N(n)$



A fixed point $z^* = (x^*, y^*)$ of the map M satisfies $M(z^*) = z^*$, making it a period-1 trajectory. This point is classified as a saddle if the Jacobian matrix of M evaluated at z^* , $DM(z^*)$, has real eigenvalues $\{\lambda_s, \lambda_u\}$ with $|\lambda_s| < 1$ (stable) and $|\lambda_u| > 1$ (unstable). Saddle points are inherently unstable: while trajectories near them may initially approach the fixed point, most will eventually diverge under successive iterations of M . The local dynamics are governed by two distinct directions defined by the eigenvectors: the contracting direction E_s , associated with λ_s , along which trajectories converge toward z^* , and the expanding direction E_u , associated with λ_u , along which trajectories diverge away from z^* .

For linear maps, these eigenvectors form straight lines intersecting at the saddle point. Initial conditions on the stable eigenvector approach z^* , while those on the unstable eigenvector move away from it. Trajectories near the saddle point follow a hyperbolic path, approaching along the stable direction and diverging along the unstable direction. A disk of initial conditions around z^* is distorted by the map into an

elongated shape, contracting along the stable direction and expanding along the unstable direction with each iteration.

For a general invertible nonlinear planar map, the stable manifold of a fixed point z^* consists of the set of points that converge to z^* under iterations of M . Formally, it is defined as:

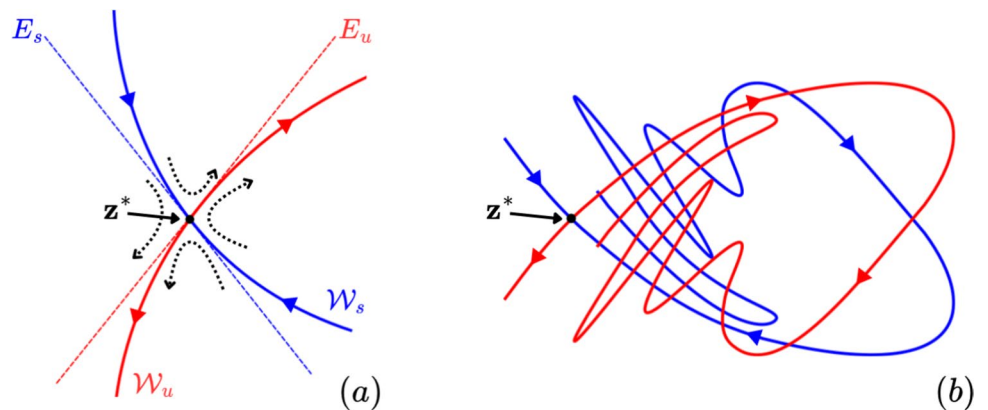
$$\mathcal{W}_s(z^*) = \{z \in \mathbb{R}^2 : M^n(z) \rightarrow z^*, \text{ as } n \rightarrow \infty\}, \tag{4}$$

where M^n is the n -th iteration of the map M . Conversely, the unstable manifold of z^* is the set of points that approach z^* under iterations of the inverse map M^{-1} :

$$\mathcal{W}_u(z^*) = \{z \in \mathbb{R}^2 : M^{-n}(z) \rightarrow z^*, \text{ as } n \rightarrow \infty\}. \tag{5}$$

At z^* , the stable manifold $\mathcal{W}_s(z^*)$ is tangent to the stable eigen-direction, while $\mathcal{W}_u(z^*)$ is tangent to the unstable eigen-direction. This is illustrated in Fig. 4(a). These manifolds are invariant curves: M maps $\mathcal{W}_s(z^*)$ and $\mathcal{W}_u(z^*)$ onto themselves, preserving their structure under iteration.

Fig. 4 Illustrations of: (a) the vicinity of a hyperbolic point z^* of a planar map, with the stable eigendirection E_s and invariant manifold \mathcal{W}_s represented in blue, and the unstable eigendirection E_u and invariant manifold \mathcal{W}_u in red; and (b) the homoclinic tangle generated by the crossings of the invariant manifolds of opposing stability



The invariant manifolds $\mathcal{W}_s(z^*)$ and $\mathcal{W}_u(z^*)$ play a crucial role in determining chaotic dynamics. A single intersection between them implies infinitely many intersections: if a point p lies on both $\mathcal{W}_s(z^*)$ and $\mathcal{W}_u(z^*)$, invariance ensures that all forward and backward iterates of p under M must also belong to both manifolds. These intersection points are called homoclinic, and they form a homoclinic orbit that asymptotically approaches z^* in both forward and backward time without ever reaching it. The resulting geometry, a fractal-like web of infinitely folded manifolds, is termed a homoclinic tangle.

Within this tangle, illustrated in Fig. 4(b), trajectories undergo repeated stretching along $\mathcal{W}_u(z^*)$ and folding along $\mathcal{W}_s(z^*)$, a mechanism that is formalized in Smale’s horseshoe map. This process embeds a Cantor set of chaotic trajectories and infinitely many UPOs of all periods. The horseshoe structure exhibits three hallmarks of chaos: sensitive dependence on initial conditions (exponential divergence of nearby trajectories), topological mixing (trajectories eventually explore the entire invariant set), and dense UPOs (unstable periodic points lie arbitrarily close to any chaotic trajectory). Analogous dynamics emerge in heteroclinic orbits, formed when $\mathcal{W}_s(z_1^*)$ of one saddle point intersects $\mathcal{W}_u(z_2^*)$ of another saddle point. However, two constraints prevent inconsistencies. First, self-intersections are forbidden: $\mathcal{W}_s(z^*)$ cannot cross itself, nor can $\mathcal{W}_u(z^*)$, as this would violate the uniqueness of solutions under M . Second, same-stability manifold crossings are prohibited: $\mathcal{W}_s(z_1^*)$ cannot intersect $\mathcal{W}_s(z_2^*)$, and $\mathcal{W}_u(z_1^*)$ cannot intersect $\mathcal{W}_u(z_2^*)$, for distinct saddle points z_1^*, z_2^* .

Homoclinic or heteroclinic intersections are necessary conditions for chaotic dynamics in both permanent chaos (supported by attractors) and transient chaos. For chaotic attractors, these homoclinic/heteroclinic structures are embedded within the attractor itself. In transient chaos, the chaotic dynamics originate from a non-attracting invariant set known as a chaotic saddle. A chaotic saddle exhibits sensitive dependence on initial conditions but, unlike chaotic attractors, does not permanently confine trajectories. Nearby orbits exhibit transient chaotic behavior, following the saddle’s unstable manifold temporarily before escaping to attractors or diverging. This set is formed through homoclinic and heteroclinic tangles between stable and unstable manifolds of saddle points. Although trajectories starting exactly on the saddle remain there indefinitely, its measure-zero nature in phase space (occupying no area) makes direct observation impossible: Random initial conditions have zero probability of lying precisely on the saddle. Its existence is instead inferred through dynamical signatures like transient chaos, where trajectories approach along stable manifolds, exhibit chaotic evolution near the saddle, then escape along unstable manifolds. The escape rate κ introduced in (2) provides a quantitative characterization of this transient behavior.

There are different numerical methods to determine chaotic saddles [1, 26, 30, 31]. An intuitive method is based on the observation that a chaotic saddle contains a dense set of UPOs. After identifying a single UPO, its invariant manifolds are computed. Intersections between these manifolds approximate subsets of the chaotic saddle [1]. While intuitive, the method becomes computationally prohibitive for high-resolution saddles due to the exponential growth of required manifold segments, necessitating advanced interpolation and adaptive refinement techniques. A computationally efficient alternative is the sprinkler method [1, 30], based on following an ensemble of trajectories and selecting segments that remain in the vicinity of the chaotic saddle; other advantages of this method are that it is simple to implement and approximates the saddle through homoclinic intersections across multiple unstable orbits. Yet another alternative is the PIM triple method [26], which constructs a single arbitrarily long trajectory near the chaotic saddle; the resulting trajectory is well-suited for computing dynamical invariants [1] like Lyapunov exponents or fractal dimensions, which characterize the saddle’s chaotic properties. In this work, we used the PIM triple method to approximate the chaotic saddles. The details of the algorithm are presented in Appendix A.

To analyze the results from the previous section in the context of invariant manifolds and chaotic saddles, we begin by identifying the fixed points of the Hénon map. The fixed point condition $M(z^*) = z^*$ yields two solutions:

$$z_{\pm}^* = (x_{\pm}^*, y_{\pm}^*) = \left(\frac{(b-1) \pm \sqrt{(b-1)^2 + 4a}}{2}, x_{\pm}^* \right), \tag{6}$$

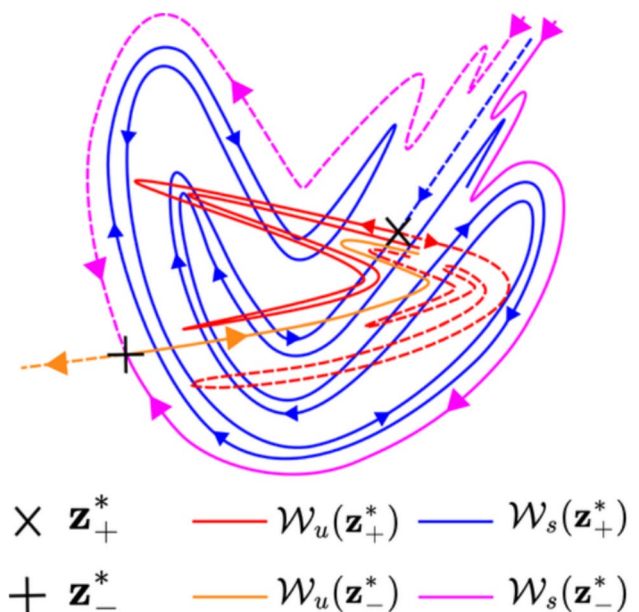


Fig. 5 Schematic of invariant manifolds in the Hénon map. The stable manifold $\mathcal{W}_s(z_+^*)$ (pink curves) forms the boundary of the trapping region R , which encloses z_+^* and its manifolds $\mathcal{W}_{s,u}(z_+^*)$ (blue/red)

and, for the parameter sets considered throughout this work, they are both real and correspond to saddle points.

Figure 5 illustrates key qualitative features of the saddle fixed points in the Hénon map. The two branches of the stable manifold $\mathcal{W}_s(z_-^*)$, shown as solid and dashed pink curves, form the boundary of the trapping region R . This region R contains the saddle point z_+^* along with its stable and unstable manifolds, $\mathcal{W}_s(z_+^*)$ and $\mathcal{W}_u(z_+^*)$. Both branches of $\mathcal{W}_s(z_-^*)$ tend asymptotically toward infinity under iterations of the inverse map. The stable manifold $\mathcal{W}_s(z_+^*)$ exhibits distinct behaviors: one branch (blue dashed curve) escapes to infinity under the inverse map, while the other (blue solid curve) oscillates, weaving around the first branch as it asymptotically approaches $\mathcal{W}_s(z_-^*)$. Both branches of the unstable manifold $\mathcal{W}_u(z_+^*)$ lie entirely within R ; they intersect $\mathcal{W}_s(z_+^*)$, creating the intricate homoclinic tangle characteristic of chaotic dynamics. Finally, for the unstable manifold $\mathcal{W}_u(z_-^*)$, one branch (dashed orange curve) escapes to $-\infty$, while the other branch (solid orange curve) remains confined within R , asymptotically approaching $\mathcal{W}_u(z_+^*)$. Following the nomenclature from Ref. [32], we call $\mathcal{W}_u(z_-^*) \cap \mathcal{W}_s(z_+^*)$ inner heteroclinic points, and $\mathcal{W}_s(z_-^*) \cap \mathcal{W}_u(z_+^*)$ outer heteroclinic points. In the diagram of Fig. 5, $\mathcal{W}_s(z_-^*) \cap \mathcal{W}_u(z_+^*) = \emptyset$. The role of outer heteroclinic points will be discussed in Section 4.

We compute finite segments of their invariant manifolds using the algorithm from Ref. [25]. This method iterates local linear approximations of the manifolds forward

(unstable) or backward (stable) in time, refining the curves with interpolation to preserve resolution¹. Results for $a = 1.22$ and $a = 1.23$ are shown in Fig. 6(a) and (c), respectively. Following the symbols and color-coding of the diagram in Fig. 5, the fixed point z_+^* (marked by “x”) displays its stable manifold ($\mathcal{W}_s(z_+^*)$) in blue and unstable manifold ($\mathcal{W}_u(z_+^*)$) in red; and the fixed point z_-^* (marked by “+”) displays its stable manifold ($\mathcal{W}_s(z_-^*)$) in pink and unstable manifold ($\mathcal{W}_u(z_-^*)$) in orange. Homoclinic intersections between these manifolds indicate chaotic behavior in the phase space. Comparing Fig. 6(c) with Fig. 3(b), we observe that the patterns revealed by the lifetime projection align with the geometry of the stable manifold.

Figure 6(b) shows the chaotic attractor for $a = 1.22$ (same parameter as in panel (a)). At the resolution of the plot it is indistinguishable from the unstable manifold $\mathcal{W}_u(z_+^*)$, drawn as the red curve in Fig. 6(a). More precisely, the attractor is the closure [32, 33] of $\mathcal{W}_u(z_+^*)$: the manifold together with all of its accumulation points (limit points of sequences on the manifold). Under iteration, the manifold is repeatedly stretched and folded, so its images come arbitrarily close to many locations in phase space; the closure captures both the original curve and these limit points, yielding the full attractor. Although $\mathcal{W}_u(z_+^*)$ itself is one-dimensional, the resulting chaotic attractor has a non-integer (fractal) dimension greater than one [34, 35].

Figure 6(d) displays the chaotic saddle (black) along with the periodic attractor (red) for $a = 1.23$. Comparison with transient trajectories in Fig. 2(b) reveals that chaotic transients first follow the chaotic saddle before converging to the periodic attractor governing asymptotic dynamics.

From Fig. 6(a) and (c) alone, one cannot distinguish whether $\mathcal{W}_u(z_+^*)$ forms a chaotic attractor or contributes to a chaotic saddle via homoclinic intersections. In Section 4, we analyze how attractors evolve with parameter a and present conditions for the unstable manifold to form a chaotic attractor.

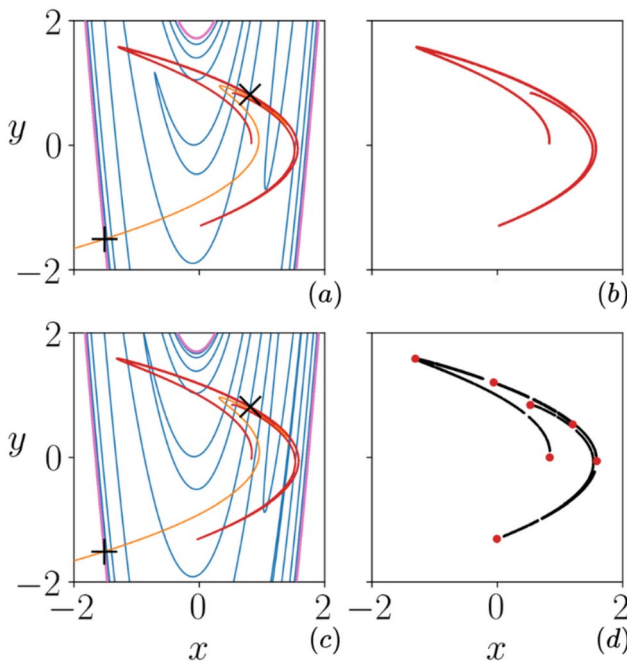


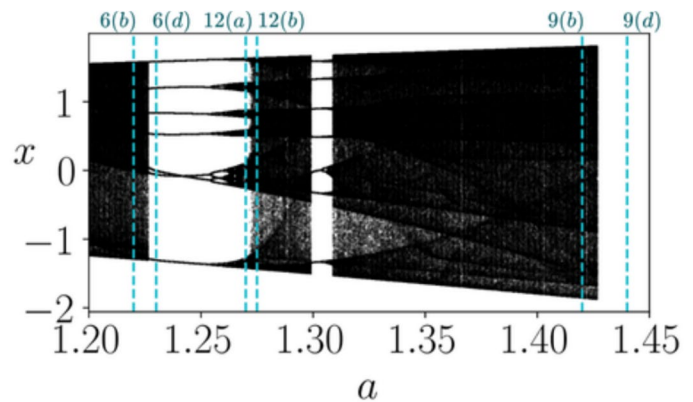
Fig. 6 Stable/unstable manifolds and chaotic sets in the Hénon map. (a) Invariant manifolds at $a = 1.22$: z_+^* (x; blue/red), z_-^* (+; pink/orange). (b) Chaotic attractor for $a = 1.22$. (c) Manifolds for $a = 1.23$. (d) Chaotic saddle (black) and periodic attractor (red) for $a = 1.23$

4 Crises and Periodic Windows

A commonly used method for visualizing how the attractor of a dynamical system evolves with changes in a parameter is the bifurcation diagram [1–4]. In such diagrams, a coordinate of the attractor is plotted against a system parameter, revealing qualitative changes in the system’s asymptotic behavior. Figure 7 presents a bifurcation diagram for the Hénon map, constructed with the parameter $b = 0.3$ and

¹ The refinement parameters considered for the method were: maximum chord length between consecutive nodes $l_c = 10^{-2}$ and maximum inter-secant angle between consecutive chords $\theta_c = 5$. For details on the method, see Ref. [25].

Fig. 7 Bifurcation diagram for $b = 0.3$. The vertical lines correspond to the values of a utilized in the indicated figures of chaotic sets



$a \in [1.2, 1.45]$. The construction followed this procedure: starting from an arbitrarily chosen non-diverging initial condition $x_0 = y_0 = 0.1$ at $a = 1.2$, the system was iterated 10^4 times, and only the final 100 x -values were plotted to eliminate any transient effects. Subsequently, the parameter a was incremented in small steps of approximately 10^{-4} , and for each step, 10^4 iterations were performed with the final 100 x -values plotted. This process continued until the upper bound of the parameter range was reached.

The term bifurcation denotes a qualitative change in a system’s attractors as parameters vary. Figure 7 shows the bifurcation diagram for the Hénon map, revealing three key features: (1) Chaotic attractors appear as densely filled x -values in certain a intervals; (2) Periodic windows interrupt these chaotic regimes, where periodic attractors undergo period-doubling cascades back to chaos; and (3) A sudden

attractor disappearance occurs at critical $a_{BC} \approx 1.43$, indicating a boundary crisis [1–3, 27, 28] where the chaotic attractor is destroyed and replaced by a chaotic saddle.

In a boundary crisis, the chaotic attractor collides with its basin boundary, enabling trajectories to escape the trapping region R . As previously established, the boundary of R is defined by $\mathcal{W}_s(z_-^*)$, while the chaotic attractor is the closure of $\mathcal{W}_u(z_+^*)$. The boundary crisis occurs when these invariant manifolds intersect, creating heteroclinic points at $\mathcal{W}_s(z_-^*) \cap \mathcal{W}_u(z_+^*)$. Figure 8 illustrates the escape mechanism: Points that escape R via $\mathcal{W}_u(z_+^*)$ subsequently follow the outer branch of $\mathcal{W}_u(z_-^*)$ toward $-\infty$. After the crisis, the homoclinic points $\mathcal{W}_s(z_-^*) \cap \mathcal{W}_u(z_+^*)$ compose the chaotic saddle that governs the chaotic transient before the trajectories diverge.

For parameters near the values considered in Hénon’s original work [18] ($b = 0.3, a = 1.4$), it is proven that the attractor is the closure of $\mathcal{W}_u(z_+^*)$, and is bounded and contains homoclinic points [33]. Previously, it had been suggested that if the unstable manifold has homoclinic points, no outer heteroclinic points, and is bounded, then its closure is a chaotic attractor [32].

More generally, when the chaotic attractor is a uniformly hyperbolic set [2], the attractor is exactly the closure of an unstable manifold [36]. “Uniformly hyperbolic” means that on the invariant set Λ every point $x \in \Lambda$ has stable and unstable subspaces, $E_s(x)$ and $E_u(x)$, and the dynamics contracts along E_s and expands along E_u at uniform exponential rates that do not depend on x . Under these conditions one can show that the attractor is the closure of the unstable manifold of a periodic orbit, however, it is often conjectured from numerical observations that even for non-hyperbolic systems the chaotic attractor is the closure of an unstable manifold [37–39].

We note that the Hénon map is not uniformly hyperbolic for all parameters [1, 2, 40]: its stable and unstable manifolds can become tangent, and at those points $E_s(x)$ and $E_u(x)$ coincide, generating nonhyperbolicity. Nonhyperbolicity mainly affects two aspects of our study. First, the shadowing

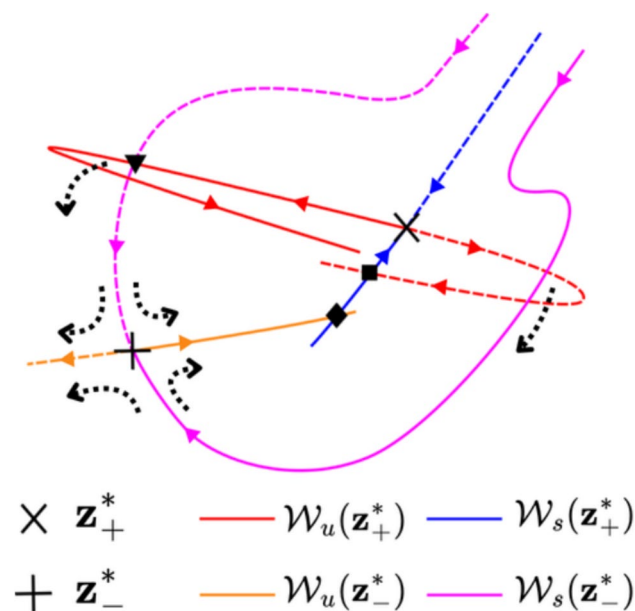


Fig. 8 Schematic of the mechanism generating escape of points from the trapping region R , due to outer heteroclinic points $\mathcal{W}_s(z_-^*) \cap \mathcal{W}_u(z_+^*)$ after the boundary crisis. The symbol \blacksquare indicates a homoclinic point, \blacktriangledown an outer heteroclinic point, and \blacklozenge an inner heteroclinic point

lemma [41, 42], which guarantees that every noisy or numerical pseudotrajectory is exactly shadowed for all time by a true trajectory, requires uniform hyperbolicity and therefore does not generally apply to the Hénon map. Nevertheless, rigorous computer-assisted studies of nonhyperbolic systems such as the logistic map and the Hénon map have shown that double-precision pseudotrajectories are typically shadowed by exact orbits for very long but finite times [43–45]. The length of a numerical trajectory for which shadowing is guaranteed is about 10^8 iterations for systems whose tangencies are the source of nonhyperbolicity.

Second, certain types of nonhyperbolic sets can lead to a power-law decay of the survival probability, thus making (2) and (3) inaccurate. This is the case, for instance, in systems with unstable dimension variability [46], where unstable periodic orbits embedded in the chaotic set have distinct number of unstable eigendirections; and can also happen in leaky Hamiltonian systems [47, 48], where non-hyperbolicity can arise if the chaotic saddle is adjacent to KAM islands and cantori. Despite nonhyperbolicity for some parameters due to manifold tangencies, the hyperbolic points of the Hénon map chaotic saddles dominate the transient dynamics, leading to the exponential decay of the survival probability.

Figure 9(a) shows the invariant manifolds of the fixed points for $a = 1.42$, before the boundary crisis, and panel (b) exhibits the chaotic attractor. We note that the chaotic attractor lies very close to its basin boundary, determined by the stable

manifold of z_-^* , shown in pink, indicating the system is near the crisis point in parameter space. In Fig. 9(c), for $a = 1.44$, we have the invariant manifolds after the crisis. Notice how the unstable manifold of z_+^* , shown in red, crosses the stable manifold of z_-^* . In panel (d), we show the chaotic saddle that supports the transient chaotic dynamics after the crisis.

To observe the transient dynamics after the boundary crisis, Fig. 10(a) shows the time series of the x variable for two nearby initial conditions. For clarity, only every 7 iterates are shown. The one in blue oscillates irregularly for approximately 800 iterates before diverging, while the second one, shown in orange, diverges after approximately 200 iterates. The full orbits are shown in panel (b), with the initial conditions marked by the blue \times and orange $+$ signs. The distance between them is on the order of 10^{-15} . Once again, the sensitivity to initial conditions is observed, as nearby initial conditions have different transient lifetimes. The chaotic transient behavior is distributed along the region of the chaotic saddle, as can be seen by comparing with Fig. 9(c). Figure 10(c) shows the survival curve. It was computed using 10^8 initial conditions uniformly distributed in the region $|x| < 2$ and $|y| < 2$. The exponential fit with $n_{min} = 30$ and $n_{max} = 1500$ estimates the escape rate as $\kappa = 9.32917755 \times 10^{-3} \pm 5.0 \times 10^{-8}$ and the average transient lifetime as $\tau = 107.19059 \pm 5.8 \times 10^{-4}$. The projection of survival times in phase space is shown in panel (d).

We now analyze the periodic windows observed in Fig. 7. Each window initiates with an embedded saddle-node bifurcation [49] that simultaneously creates an attracting period- k orbit ($z_{k,A}^*$) and a saddle period- k orbit ($z_{k,U}^*$). The dynamics near these orbits exhibit the manifold structures [32]: one branch of $\mathcal{W}_u(z_{k,U}^*)$ is attracted toward $z_{k,A}^*$; and $\mathcal{W}_s(z_{k,U}^*)$ encloses a region containing both $z_{k,A}^*$ and the attracted branch of $\mathcal{W}_u(z_{k,U}^*)$.

When $\mathcal{W}_s(z_{k,U}^*)$ intersects the chaotic attractor (equivalent to intersecting $\mathcal{W}_u(z_+^*)$), the resulting heteroclinic points function analogously to the outer heteroclinic points, described previously for the boundary crisis. This intersection triggers the conversion of the chaotic attractor into a chaotic saddle. Figure 11 illustrates this attractor destruction mechanism via saddle-node bifurcation.

The first vertical line in Fig. 7 marks $a = 1.22$, which corresponds to the chaotic attractor shown in Fig. 6(b). As a increases, the chaotic attractor is abruptly replaced by a period-7 attractor at the saddle-node bifurcation. The second vertical line, at $a = 1.23$, corresponds to this periodic attractor and the coexisting associated chaotic saddle, as illustrated in Fig. 6(d). The period-7 attractor then undergoes a period-doubling cascade [2, 3], leading to a chaotic attractor composed of seven disconnected pieces, known as bands. At $a = 1.27$, marked by the third vertical line, the phase space

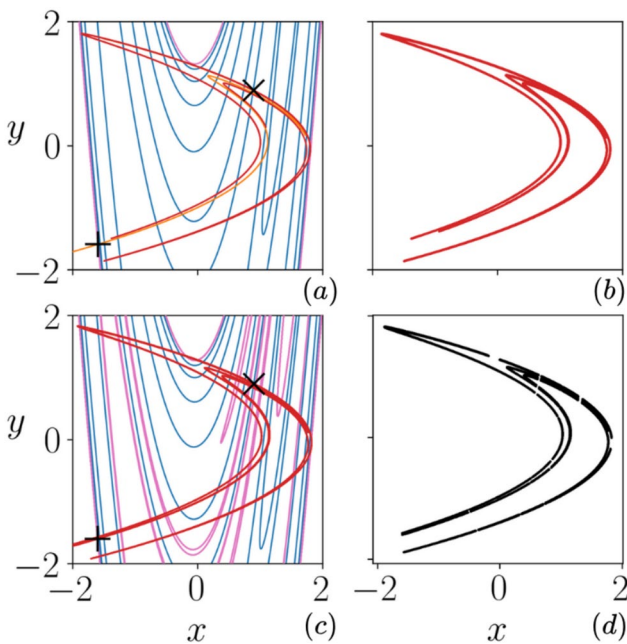


Fig. 9 For $a = 1.42 < a_{BC}$, before the interior crisis, (a) stable (blue and pink) and unstable (red and orange) manifolds of the fixed points. (b) Chaotic attractor. For $a = 1.44 > a_{BC}$, after the interior crisis, (c) the invariant manifolds and (d) the chaotic saddle

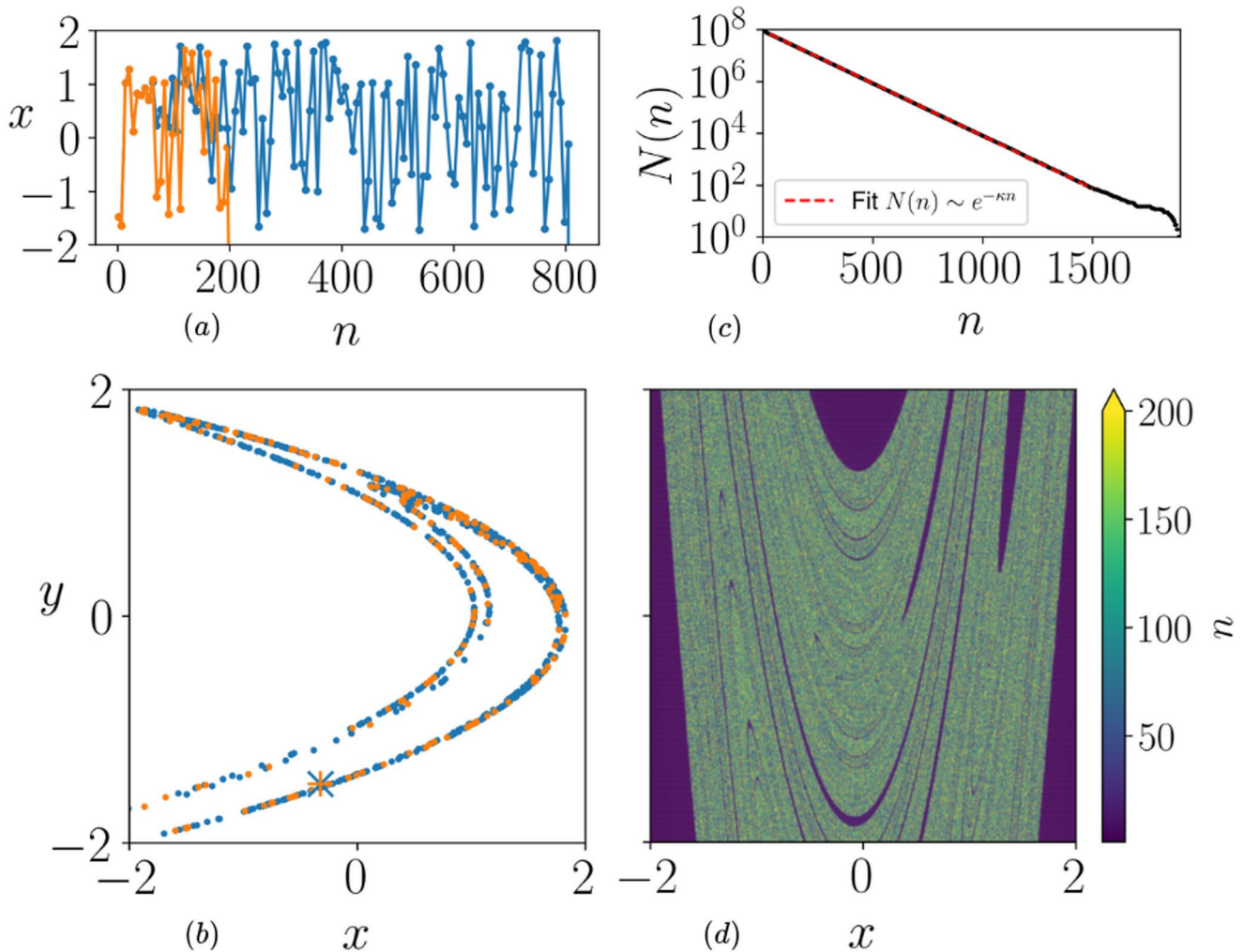


Fig. 10 For $a = 1.44$, (a) time evolution of the x coordinate for two initial conditions, each seventh iteration is shown. In blue, a long-lived initial condition that diverged after approximately 800 iterations. In orange, the initial condition was shifted by 10^{-15} , and the trajectory diverged after approximately 200 iterations. (b) Evolution of the orange and blue initial points, indicated

by the '+' and 'x' symbols, respectively. (c) Number of surviving trajectories as a function of the number of iterations, the exponential fitting in furnished $\kappa = 9.32917755 \times 10^{-3} \pm 5.0 \times 10^{-8}$ and $\tau = 107.19059 \pm 5.8 \times 10^{-4}$. (d) Projection of survival times in the phase space

(Fig. 12(a)) shows the banded chaotic attractor in red and the chaotic saddle in black. As a continues to increase and exceeds a critical value a_{IC} , the seven-band chaotic attractor abruptly transitions into a single, much larger chaotic attractor. The fourth vertical line, at $a = 1.275$, corresponds to the resulting attractor shown in Fig. 12(b). The mechanism behind this transformation is an interior crisis [1–3, 27, 28], where the banded chaotic attractor collides with the chaotic saddle. As a result, the UPOs that previously belonged to the chaotic saddle are incorporated into the attractor, along with newly created unstable orbits.

The whole interval between the saddle-node bifurcation, that replaces a large chaotic attractor by a chaotic saddle, and the interior crisis, at which a large chaotic attractor is recovered, is known as a periodic window. For any periodic

window, a generic feature is that a chaotic saddle exists throughout the window, so chaotic transients are observed. A second periodic window is observed starting at $a \approx 1.3$. In fact, in parameter regions where a chaotic attractor arises, the periodic windows are dense [1, 2]; this means that, given a parameter \bar{a} for which the attractor is chaotic, one can always find a periodic window in the interval $[\bar{a} - \epsilon, \bar{a} + \epsilon]$, no matter how small ϵ is.

5 Concluding Remarks

In this work we consider the Hénon map, a dissipative and invertible 2D map. This system is representative of dissipative three-dimensional flows, as those are invertible due to

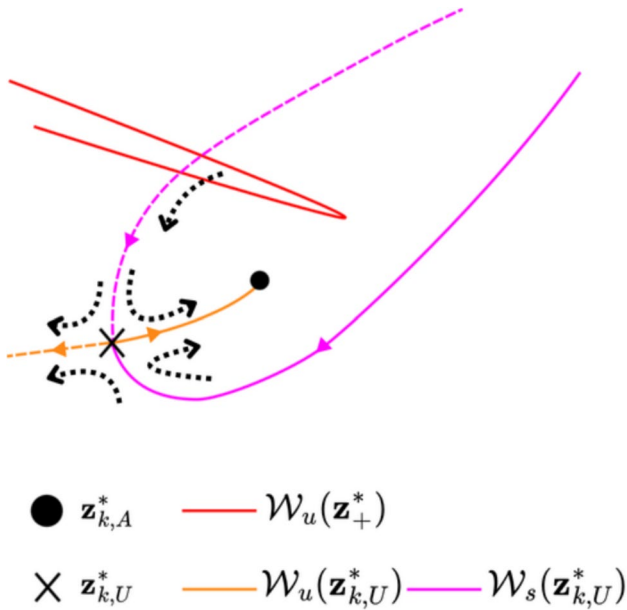


Fig. 11 Schematic of the destruction of a chaotic attractor by the k -periodic orbits created in a saddle-node bifurcation

the uniqueness of solutions and can be analyzed through a Poincaré map [4]. We demonstrate that long chaotic transients are organized by a non-attracting chaotic saddle formed by homoclinic and heteroclinic tangles of stable and unstable manifolds. We quantify this saddle by the escape rate κ , inferred from the exponential decay of the survival probability, which measures how quickly typical trajectories leave the saddle’s vicinity. Long-lived trajectories approach the saddle along its stable manifold W_s and depart along the unstable manifold W_u toward an asymptotic state.

Chaotic saddles commonly appear inside periodic windows. There, a saddle–node bifurcation creates a stable period- k orbit together with an unstable saddle orbit; intersections of the period- k saddle’s stable manifold with the surrounding chaotic attractor convert the attractor into a chaotic saddle. As an example, we analyzed the period-7 window, for which the periodic attractor undergoes a

period-doubling cascade, and an interior crisis reincorporates the chaotic saddle into the banded chaotic attractor, producing a larger chaotic attractor. We also observe long chaotic transients after a boundary crisis, when the chaotic attractor collides with its basin boundary and is converted into a chaotic saddle.

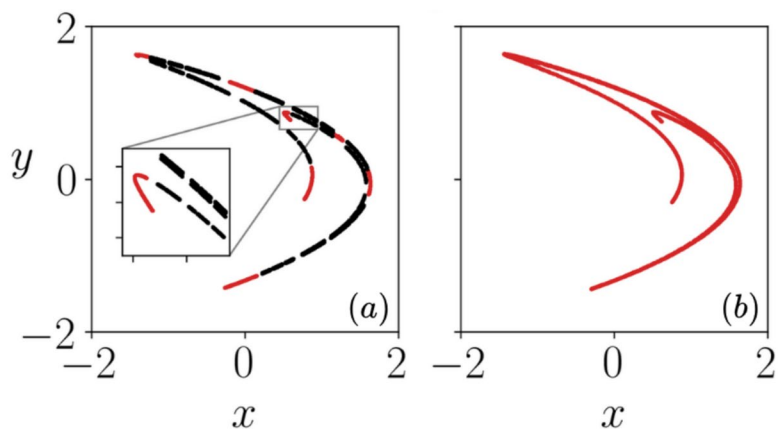
In contrast, in noninvertible systems such as one-dimensional maps (e.g. the Logistic map), transient chaos is supported by another type of nonattracting set: the chaotic repeller [1], which possesses only unstable manifolds. The dynamical difference between a saddle and a repeller is that long-lived chaotic transients can only start from a neighborhood of the repeller, while for saddles, it can start from a neighborhood of the stable manifold, which is typically a larger set.

Another type of dynamical system not treated here is that of conservative or Hamiltonian systems [50, 51]. In this type of system, the phase space volume is preserved under the time evolution, so there are no attractors. However, asymptotic states can still be defined if a hole or leak is introduced in the phase space of a closed system [52–55], or in the case of open systems where trajectories naturally escape [56–58]. The solutions can behave chaotically before reaching those states if a chaotic saddle is present in the phase space. This phenomenon is known as chaotic scattering [1, 59].

Chaotic saddles are also observed across high-dimensional systems. For instance, in spatially extended systems such as a lattice of coupled oscillators or maps, chaotic saddles are associated with long transients [60, 61]. In complex networks, they are responsible for self-induced switching between spatiotemporal patterns [62], and can impact the synchronization states due to dynamical trapping [63, 64].

To conclude, our objective in this article has been to present transient chaos — which is less widely known than the permanent chaos associated with attractors — and to present a concise, self-contained account of its mechanisms, diagnostics, and implications. By emphasizing the role of chaotic saddles and invariant manifolds, we aim to make

Fig. 12 (a) Chaotic attractor (red) and coexisting chaotic saddle (black) for $a = 1.27$, before the interior crisis; and (b) chaotic attractor for $a = 1.275$, after the interior crisis. At a critical value $1.27 < a_{IC} < 1.275$, the banded chaotic attractor collides with the chaotic saddle, resulting in an enlarged chaotic attractor



transient chaos part of the standard vocabulary in physics. Recognizing when chaos is transient rather than sustained is practically important: it controls finite-time statistics and escape rates, organizes transport and mixing, and shapes the interpretation of experiments and simulations. We hope this overview helps readers identify transient chaos in their own systems and provides a foundation for further theoretical, numerical, and experimental work.

A The PIM Triple Method

The PIM triple method [26] is a numerical procedure for computing a single, arbitrarily long trajectory that approximates a chaotic saddle Λ . It is based on the observation that initial conditions closer to the stable manifold of Λ exhibit longer transient lifetimes: they require more iterations to leave a trapping region R or converge to an attractor.

The algorithm starts with a line segment $\overline{A_0B_0}$ that intersects the stable manifold of Λ ; a lifetime projection (e.g., Fig. 3(c)) can be used to guide this choice since the longest-lived trajectories are near the stable manifold, and the projection highlights its geometry. The segment is refined as follows. Uniformly distribute $N = 10^3$ points on $\overline{A_0B_0}$ and compute their lifetimes. Identify three consecutive points (A_1, C_1, B_1) such that the middle point C_1 has a longer lifetime than its two neighbors. Replace the original segment by $\overline{A_1B_1}$ and repeat the refinement procedure recursively, producing segments $\overline{A_2B_2}, \overline{A_3B_3}, \dots$, until a segment $\overline{A_nB_n}$ of length smaller than $\delta = 10^{-8}$ is obtained. The triple (A_n, C_n, B_n) is then called a *proper interior maximum (PIM) triple*.

Define $I_0 = \overline{A_nB_n}$. The points of the PIM triple are iterated under the map M , yielding a new triple $(M(A_n), M(C_n), M(B_n))$ and the associated interval $I_1 = \overline{M(A_n)M(B_n)}$. If $|I_1| > \delta$, apply the refinement step to I_1 to obtain a new PIM triple with interval length smaller than δ . If $|I_1| \leq \delta$, iterate the triple further until the interval becomes larger than δ , at which point the refinement is restarted. Repeating this cycle of iterating the current PIM triple and refining whenever the interval length exceeds δ , produces a sequence of PIM triples whose intervals remain of order δ in size.

The set of middle points $\{C_k\}$ generated in this way approximates a typical trajectory on the chaotic saddle. This numerically constructed orbit is often referred to as a *straddle trajectory*: it remains within a distance of order δ from Λ for arbitrarily long times, thereby providing an effective approximation of the saddle dynamics. The chaotic saddles in this work were approximated by trajectories with 5×10^5 points, precision $\delta = 10^{-8}$ and $N = 10^3$ initial conditions for the refining steps.

Acknowledgements This study was supported by the São Paulo Research Foundation (FAPESP), Brazil, under Grants Nos. 2024/05700-5, 2024/04557-4; and by the National Council for Scientific and Technological Development (CNPq), Brazil, under Grant No. 304616/2021-4.

Author Contributions R.S.B.: conceptualization, investigation, software, writing - original draft and editing. I.L.C.: conceptualization, investigation, writing - review.

Funding The Article Processing Charge (APC) for the publication of this research was funded by the Coordenação de Aperfeiçoamento de Pessoal de Nível Superior - Brasil (CAPES) (ROR identifier: 00x0ma614).

Data Availability The computer code to generate the data that support the findings of this study will be openly available in the Oscillations Control Group Data Repository, <http://henon.if.usp.br/OscilControlData/>.

Declarations

Competing Interests The authors declare no competing interests.

Open Access This article is licensed under a Creative Commons Attribution 4.0 International License, which permits use, sharing, adaptation, distribution and reproduction in any medium or format, as long as you give appropriate credit to the original author(s) and the source, provide a link to the Creative Commons licence, and indicate if changes were made. The images or other third party material in this article are included in the article's Creative Commons licence, unless indicated otherwise in a credit line to the material. If material is not included in the article's Creative Commons licence and your intended use is not permitted by statutory regulation or exceeds the permitted use, you will need to obtain permission directly from the copyright holder. To view a copy of this licence, visit <http://creativecommons.org/licenses/by/4.0/>.

References

1. Y.-C. Lai, T. Tél, *Transient Chaos* (Springer, New York, NY, 2011)
2. E. Ott, *Chaos in Dynamical Systems*, 2nd edn. (Cambridge University Press, Cambridge, 2002)
3. K.T. Alligood, T.D. Sauer, J.A. Yorke, *Chaos: An Introduction to Dynamical Systems* (Springer, Berlin, Heidelberg, 1997)
4. M. Cattani, I.L. Caldas, S.L. de Souza, K.C. Iarosz, Deterministic chaos theory: Basic concepts. *Rev. Bras. Ens. Fis.* **39**(1), e4503 (2016)
5. S.K. Scott, B. Peng, A.S. Tomlin, K. Showalter, Transient chaos in a closed chemical system. *J. Chem. Phys.* **94**(2), 1134–1140 (1991)
6. J. Wang, P.G. Soerensen, F. Hynne, Transient period doublings, torus oscillations, and chaos in a closed chemical system. *J. Phys. Chem.* **98**(3), 725–727 (1994)
7. J. Zhao, Y. Chen, J. Wang, Transient complex oscillations in a closed chemical system with coupled autocatalysis. *J. Chem. Phys.* **122**(11), 114514 (2005)
8. E.I. Butikov, Regular and chaotic motions of the parametrically forced pendulum: Theory and simulations, in *Computational Science — ICCS 2002*. ed. by P.M.A. Sloot, A.G. Hoekstra, C.J.K. Tan, J.J. Dongarra (Springer, Berlin, Heidelberg, 2002), pp. 1154–1169

9. R.W. Leven, M. Selent, Construction and quantitative characterization of a chaotic saddle from a pendulum experiment. *Chaos, Solitons Fractals* **4**(12), 2217–2222 (1994)
10. A.S. de Paula, M.A. Savi, F.H.I. Pereira-Pinto, Chaos and transient chaos in an experimental nonlinear pendulum. *J. Sound Vib.* **294**(3), 585–595 (2006)
11. H.G.L. Schwefel, N.B. Rex, H.E. Tureci, R.K. Chang, A.D. Stone, T. Ben-Messaoud, J. Zyss, Dramatic shape sensitivity of directional emission patterns from similarly deformed cylindrical polymer lasers. *J. Opt. Soc. Am. B* **21**(5), 923–934 (2004)
12. E.G. Altmann, Emission from dielectric cavities in terms of invariant sets of the chaotic ray dynamics. *Phys. Rev. A* **79**(1), 013830 (2009)
13. M. Gorman, P.J. Widmann, K.A. Robbins, Chaotic flow regimes in a convection loop. *Phys. Rev. Lett.* **52**(25), 2241–2244 (1984)
14. M. Gorman, P.J. Widmann, K.A. Robbins, Nonlinear dynamics of a convection loop: A quantitative comparison of experiment with theory. *Physica D* **19**(2), 255–267 (1986)
15. Y. Wang, J. Singer, H.H. Bau, Controlling chaos in a thermal convection loop. *J. Fluid Mech.* **237**, 479–498 (1992)
16. P.J. Widmann, M. Gorman, K.A. Robbins, Nonlinear dynamics of a convection loop II. Chaos in laminar and turbulent flows. *Physica D* **36**(1–2), 157–166 (1989)
17. E.N. Lorenz, Deterministic nonperiodic flow. *J. Atmos. Sci.* **20**(2), 130–141 (1963)
18. M. Hénon, A two-dimensional mapping with a strange attractor. *Commun. Math. Phys.* **50**(1), 69–77 (1976)
19. J.A.C. Gallas, Structure of the parameter space of the Hénon map. *Phys. Rev. Lett.* **70**(18), 2714–2717 (1993)
20. S. Kraut, U. Feudel, Noise-induced escape through a chaotic saddle: Lowering of the activation energy. *Physica D* **181**(3–4), 222–234 (2003)
21. S. Kraut, U. Feudel, Enhancement of noise-induced escape through the existence of a chaotic saddle. *Phys. Rev. E* **67**(1), 015204 (2003)
22. S. Kraut, U. Feudel, Multistability, noise, and attractor hopping: The crucial role of chaotic saddles. *Phys. Rev. E* **66**(1), 015207 (2002)
23. E.L. Rempel, A.C.-L. Chian, E.E.N. Macau, R.R. Rosa, Analysis of chaotic saddles in low-dimensional dynamical systems: The derivative nonlinear Schrödinger equation. *Physica D* **199**(3–4), 407–424 (2004)
24. R. Simile Baroni, R. Egydio de Carvalho, I.L. Caldas, R.L. Viana, P.J. Morrison, Chaotic saddles and interior crises in a dissipative nontwist system. *Phys. Rev. E* **107**(2), 024216 (2023)
25. D. Ciro, I.L. Caldas, R.L. Viana, T.E. Evans, Efficient manifolds tracing for planar maps. *Chaos* **28**(9), 093109 (2018)
26. H.E. Nusse, J.A. Yorke, A procedure for finding numerical trajectories on chaotic saddles. *Physica D* **36**(1–2), 137–156 (1989)
27. C. Grebogi, E. Ott, J.A. Yorke, Chaotic attractors in crisis. *Phys. Rev. Lett.* **48**(22), 1507–1510 (1982)
28. C. Grebogi, E. Ott, J.A. Yorke, Crises, sudden changes in chaotic attractors, and transient chaos. *Physica D* **7**(1–3), 181–200 (1983)
29. M. Widom, D. Bensimon, L.P. Kadanoff, S.J. Shenker, Strange objects in the complex plane. *J. Stat. Phys.* **32**(3), 443–454 (1983)
30. G.H. Hsu, E. Ott, C. Grebogi, Strange saddles and the dimensions of their invariant manifolds. *Phys. Lett. A* **127**(4), 199–204 (1988)
31. D. Sweet, H.E. Nusse, J.A. Yorke, Stagger-and-step method: Detecting and computing chaotic saddles in higher dimensions. *Phys. Rev. Lett.* **86**(11), 2261–2264 (2001)
32. C. Simó, On the Hénon-Pomeau attractor. *J. Stat. Phys.* **21**(4), 465–494 (1979)
33. M. Benedicks, L. Carleson, The dynamics of the Hénon map. *Ann. Math.* **133**(1), 73–169 (1991)
34. D.A. Russell, J.D. Hanson, E. Ott, Dimension of strange attractors. *Phys. Rev. Lett.* **45**(14), 1175–1178 (1980)
35. P. Grassberger, I. Procaccia, Measuring the strangeness of strange attractors. *Physica D* **9**(1–2), 189–208 (1983)
36. S. Smale, Differentiable dynamical systems. *Bull. Am. Math. Soc.* **73**(6), 747–817 (1967)
37. S.M. Hammel, J.V. Moloney, C.K.R.T. Jones, Global dynamical behavior of the optical field in a ring cavity. *J. Opt. Soc. Am. B* **2**(4), 552–564 (1985)
38. H.M. Osinga, Understanding the geometry of dynamics: The stable manifold of the Lorenz system. *J. R. Soc. N. Z.* **48**(2–3), 203–214 (2018)
39. A.A.P. Rodrigues, Abundance of strange attractors near an attracting periodically perturbed network. *SIAM J. Appl. Dyn. Syst.* **20**(1), 541–570 (2021)
40. Y.-C. Lai, C. Grebogi, J.A. Yorke, I. Kan, How often are chaotic saddles nonhyperbolic? *Nonlinearity* **6**, 779–797 (1993)
41. D.V. Anosov, Geodesic flows and closed Riemannian manifolds with negative curvature. *Proc. Steklov Inst. Math.* **90** (1967)
42. R. Bowen, ω -limit sets for Axiom A diffeomorphisms. *J. Differential Equations* **18** (1975)
43. S.M. Hammel, J.A. Yorke, C. Grebogi, Do numerical orbits of chaotic dynamical processes represent true orbits? *J. Complex.* **3**(2), 136–145 (1987)
44. S.M. Hammel, J.A. Yorke, C. Grebogi, Numerical orbits of chaotic processes represent true orbits. *Bull. Am. Math. Soc.* **19**(2), 465–469 (1988)
45. C. Grebogi, S.M. Hammel, J.A. Yorke, T. Sauer, Shadowing of physical trajectories in chaotic dynamics: Containment and refinement. *Phys. Rev. Lett.* **65**(13), 1527–1530 (1990)
46. E.J. Kostelich, I. Kan, C. Grebogi, E. Ott, J.A. Yorke, Unstable dimension variability: A source of nonhyperbolicity in chaotic systems. *Physica D* **109**(1–2), 81–90 (1997)
47. Y.-C. Lai, M. Ding, C. Grebogi, R. Blümel, Algebraic decay and fluctuations of the decay exponent in Hamiltonian systems. *Phys. Rev. A* **46**(8), 4661–4669 (1992)
48. A.E. Motter, Y.-C. Lai, C. Grebogi, Reactive dynamics of inertial particles in nonhyperbolic chaotic flows. *Phys. Rev. E*, **68**(5), 056307 (2003)
49. C. Robert, K.T. Alligood, E. Ott, J.A. Yorke, Explosions of chaotic sets. *Physica D* **144**(1–2), 44–61 (2000)
50. R.S. MacKay, J.D. Meiss, I.C. Percival, Transport in Hamiltonian systems. *Physica D* **13**(1–2), 55–81 (1984)
51. J.D. Meiss, Symplectic maps, variational principles, and transport. *Rev. Mod. Phys.* **64**(3), 795–848 (1992)
52. E.G. Altmann, J.S.E. Portela, T. Tél, Leaking chaotic systems. *Rev. Mod. Phys.* **85**(2), 869–918 (2013)
53. L.C. Souza, A.C. Mathias, I.L. Caldas, Y. Elskens, R.L. Viana, Fractal and Wada escape basins in the chaotic particle drift motion in tokamaks with electrostatic fluctuations. *Chaos* **33**(8), 083132 (2023)
54. E.C. da Silva, I.L. Caldas, R.L. Viana, M.A.F. Sanjuán, Escape patterns, magnetic footprints, and homoclinic tangles due to ergodic magnetic limiters. *Phys. Plasmas* **9**(12), 4917–4928 (2002)
55. T. Kroetz, M. Roberto, I.L. Caldas, R.L. Viana, Escape patterns of chaotic magnetic field lines in a tokamak with reversed magnetic shear and an ergodic limiter. *Phys. Plasmas* **15**, 092310 (2008)
56. V.M. de Oliveira, M.S. Palmero, I.L. Caldas, Measure, dimension, and complexity of the transient motion in Hamiltonian systems. *Physica D* **431**, 133126 (2021)
57. V.M. de Oliveira, D. Ciro, I.L. Caldas, Dynamical trapping in the area-preserving Hénon map. *Eur. Phys. J. Spec. Top.* **229**(8), 1507–1516 (2020)
58. T. Kovács, B. érdi, Transient chaos in the Sitnikov problem. *Celest. Mech. Dyn. Astron.* **105**(4), 289–304 (2009)

59. E. Ott, T. Tél, Chaotic scattering: An introduction. *Chaos* **3**(4), 417–426 (1993)
60. E.L. Rempel, A.C.-L. Chian, E.E.N. Macau, R.R. Rosa, Analysis of chaotic saddles in high-dimensional dynamical systems: The Kuramoto-Sivashinsky equation. *Chaos* **14**(3), 545–556 (2004)
61. Y.-C. Lai, R.L. Winslow, Geometric properties of the chaotic saddle responsible for supertransients in spatiotemporal chaotic systems. *Phys. Rev. Lett.* **74**(26), 5208–5211 (1995)
62. G. Ansmann, K. Lehnertz, U. Feudel, Self-induced switchings between multiple space-time patterns on complex networks of excitable units. *Phys. Rev. X* **6**(1), 011030 (2016)
63. E.S. Medeiros, O. Omel'chenko, U. Feudel, Transient chimera states emerging from dynamical trapping in chaotic saddles. *Chaos* **33**(9), 093115 (2023)
64. E.S. Medeiros, R.O.T. Medrano, I.L. Caldas, U. Feudel, The impact of chaotic saddles on the synchronization of complex networks of discrete-time units. *J. Phys. Complex.* **2**(3), 035019 (2021)

Publisher's Note Springer Nature remains neutral with regard to jurisdictional claims in published maps and institutional affiliations.